Optimal Inclination and Azimuth Angles of a Photovoltaic Module With Load Patterns for Improved Power System Stability

Hoonjoo Choi, Jinho Choi, Seong-Hyeon Ahn, Jin Hee Hyun, Hae-Lim Cha, Byeong-Yong Lim, and Hyung-Keun Ahn, *Member, IEEE*

***Abstract*—Globally, large-scale photovoltaic (PV) systems are being installed to achieve maximum power generation efficiency. However, this often results in severe power fluctuations, impacting the stability of the power system. To enhance the power system stability, it is crucial to effectively distribute the times of maximum power output. This can be achieved by making changes to the inclination angle and azimuth of PV modules at power plants. The modeling results indicate a prediction error of 3.65% relative to the actual measurements. To assess system stability based on each installation method, new concepts called demand gradient (DG) and demand gradient average (DGA) were introduced and analyzed using the load pattern in Metropolitan Seoul. The electricity usage was categorized into four divisions: residential (dwelling), public, service, and manufacturing. The analysis revealed that optimal inclination angles for the dwelling, public, service, and manufacturing sectors were 60°, 30°, 30°, and 15°, respectively. As for installation azimuths, the optimal values were 0°, 80°, 160°, and 230°, respectively. When both the inclination angle and azimuth were varied simultaneously, their optimal installation methods included inclination angles of 60°, 60°, 35°, and 50°, and azimuths of 330°, 210°, 230°, and 190° for the dwelling, public, service, and manufacturing sectors, respectively. Among the various scenarios, the most significant improvement in grid stability was observed in the existing south-facing installation of DGA in the dwelling sector, demonstrating a remarkable 77% reduction from 0.1 to 0.057.**

***Index Terms*—Bifacial module, demand gradient (DG), inclination and azimuth angles, peak cut, power system stability, RE100.**

Manuscript received 21 November 2023; revised 22 December 2023 and 2 February 2024; accepted 12 March 2024. Date of publication 2 April 2024; date of current version 19 April 2024. This work was supported in part by Human Resources Development Program of the Korea Institute of Energy Technology Evaluation and Planning (KETEP) grant funded by the Ministry of Trade, Industry and Energy, Republic of Korea RS-2023-00237035. *(Corresponding author: Hyung-Keun Ahn.)*

Hoonjoo Choi, Seong-Hyeon Ahn, Jin Hee Hyun, Hae-Lim Cha, Byeong-Yong Lim, and Hyung-Keun Ahn are with the Next Generation Photovoltaic Module and Power System Research Center and Department of Electrical Engineering, Konkuk University, Seoul 05029, South Korea (e-mail: hj.choi@s-teco.co.kr; assadd99@konkuk.ac.kr; l6ky4122@konkuk.ac.kr; haelim219@gmail.com; byeongyonglima@gmail.com; hkahn@konkuk.ac.kr).

Jinho Choi is with Chungbuk Technopark Next Generation Energy Center, PV Technical Center, Chungcheongbuk-do 27872, South Korea (e-mail: jhchoi@cbtp.or.kr).

Color versions of one or more figures in this article are available at https://doi.org/10.1109/JPHOTOV.2024.3380459.

Digital Object Identifier 10.1109/JPHOTOV.2024.3380459

I. Introduction

RE100 is an international commitment where businesses pledge to meet all their energy requirements through electricity generated solely from renewable resources, such as solar power. Initiated in 2014 in response to the climate crisis, this movement has garnered participation from 320 companies as of 2021, and the number continues to rise [1]. The total power consumption of Korean companies in 2021 reached 53.9 TWh, necessitating a considerable area to generate the corresponding power for RE100 [2], [3]. To tackle this challenge, research has been conducted on bifacial and shingled modules, aiming to enhance the efficiency of photovoltaic (PV) modules and explore high-efficiency power plant installation methods [4], [5]. High-efficiency power plants are commonly installed facing true south, a widespread method globally. However, the growing adoption of true southern installations has led to a misalignment between peak electricity production and peak electricity usage [6], resulting in potential disruptions to transmission lines and stable electricity supply issues [7]. In some cases, saturation of the transmission lines may even necessitate the shutdown of power plants. This issue can be improved by considering the method of installing PV modules by adjusting the east-west orientation, azimuth, and inclination angle [8]. There are a few studies that indicate that while the maximum output is 15% lower when installed in an east-west orientation compared to the traditional south-facing method, adjusting the peak electricity generation times of the PV power plant [9] can reduce the fluctuation rate of electricity in the transmission lines [10]. Therefore, it is thought that applying these characteristics to the electricity usage patterns according to the industrial structure of each city can help in the stable operation of transmission lines. Recent research has included studies on the predicting power generation amount of east-west oriented and south-facing PV modules using bifacial modules [11], and research on the optimal inclination angles and directions considering the latitude and longitude of the installation site [12]. In this study, not only for PV power plants installed in an east-west orientation but also considering the electricity usage patterns of consumers, the optimal PV module inclination angle and orientation that can improve electrical stability are presented.

This article will be described in the following order. Section II presents an explanation of the variables required to calculate

changes in solar irradiance based on the azimuth and inclination angles of PV modules. The front and rear irradiance values of bifacial PV modules were calculated, with the rear irradiance estimated using the calculated front solar irradiance and view factors. Subsequently, a prediction model for the front and back outputs of bifacial PV modules was developed using the estimated solar irradiance. Section III describes the experiments conducted to verify the accuracy of the prediction model, wherein the output was measured while varying the inclination and azimuth angles of the PV modules. In addition, the error between the measured output and the model-predicted output was analyzed. In Section IV, load patterns are analyzed and categorized based on their purposes. With this analysis, we propose the most suitable inclination and azimuth angles for PV modules to ensure power system stability. Section V presents the results and Section VI presents the conclusion and the utility of this study.

II. Modeling

This study proposes an analysis method for predicting the output of PV power plants based on the movement of the Sun. While several prediction methods exist, such as utilizing the temperature of PV modules for prediction [13], employing big data for statistical methods [14], and considering the angle between the movement of the Sun and solar modules, this study focuses on using the Sun's movement as the fundamental basis for the prediction approach.

A. Prediction of Front Irradiance According to the Movement of the Sun

The position of the Sun, as observed from Earth, is determined by various factors, including the Earth's rotation, its revolution around the Sun, and the observer's specific location, which is specified by latitude and longitude. The amount of solar radiation received by a particular surface area, known as solar irradiance, varies based on the angle between the position of the Sun and the PV modules. To predict the solar irradiance of a PV power plant considering changes in the east-west direction and the installation azimuth angle, the angle formed between the power plant and the Sun must be calculated. This calculation requires specific variables, namely the declination, altitude, and azimuth angles of the Sun.

1) Declination Angle (δ): The Sun's declination angle varies seasonally due to the Earth's axial inclination and its revolution around the Sun. This angle is represented in (1), which is a function of d and accounts for seasonal changes [15]

$$\delta = -23.45^\circ \times \cos\left(\frac{360}{365} \times (d+10)\right). \tag{1}$$

Here, d represents the days of the year, indicating the ordinal day on which the prediction is desired. It increases by one each successive day, starting from $d = 1$ for January 1 to $d = 365$ for December 31.

2) Elevation Angle: The solar altitude angle (θ) represents the angle between the Sun and the ground, and its value continuously varies based on the stationary PV modules' angle [16]

$$\theta = \sin^{-1}\left(\sin(\emptyset) \times \sin(\delta) + \cos(\emptyset) \times \cos(\delta) \times \cos(HRA)\right). \tag{2}$$

The altitude angle (θ) can be expressed using the variables $\emptyset$ (observer's latitude), δ (declination angle), and hour angle (HRA). These values can be negative or positive, where a negative solar altitude implies the Sun is below the horizon and has not yet risen, while a positive solar altitude indicates that the Sun has risen. These can be calculated using (3)–(5) [17]

$$\mathrm{HRA} = 15^\circ \left(\left(LT + \frac{TC}{60}\right) - 12\right) \tag{3}$$

$$\mathrm{TC} = 4\left(\mathrm{Longitude} - 15^\circ \times \Delta t_{\mathrm{UTC}}\right) + 9.87\sin(2B) - 7.53\cos(B) - 1.5\sin(B) \tag{4}$$

$$B = \frac{360}{365}(d - 81). \tag{5}$$

The HRA is represented in terms of local time (LT) and time correction (TC) in (3). LT indicates the time at a specific location and is expressed in a 24-h format. The TC in (4) compensates for variations in local solar time within the same time zone due to changes in longitude. Furthermore, TC can be calculated using the longitude, the difference in UTC time (Δt_{UTC}), and the time at the prediction location. The TC value uses the days of the year (B).

3) Azimuth Angle (β): Although PV power plants typically face south, they can be installed in various directions based on specific objectives. The azimuth angle of the Sun must be considered when predicting the solar irradiance of solar power plants [18]

$$\beta = \cos^{-1}\left[\frac{\sin\delta\cos\emptyset - \cos\delta\sin\emptyset\cos(\mathrm{HRA})}{\cos\theta}\right]. \tag{6}$$

The azimuth angle (β) can be calculated using (6), which involves variables such as the declination angle of the Sun, observer's latitude, HRA, and solar zenith angle. With north as the baseline at 0°, PV modules installed facing east, south, and west correspond to azimuth angles of 90°, 180°, and 270°, respectively. The amount of sunlight striking the PV modules changes according to the incidence angle, which, in turn, is affected by the azimuth and inclination angles of the PV module. The change in sunlight due to the incident angle implies a shift in the peak output time of the PV power plant.

It is essential to analyze solar irradiance based on changes in the inclination and azimuth angles to simulate comparisons of the maximum output. The variables α, β, and θ denote the inclination angle of the PV modules, the azimuth angle, and the solar altitude, respectively. The azimuth angle increases by 90° in the order of north-east-south-west, starting from 0°

$$S_{\mathrm{module}} = S_{\mathrm{incident}}\left[\cos\theta\sin\alpha\cos(\Delta\beta) + \sin\theta\cos\alpha\right]. \tag{7}$$

A predictive equation that changes according to the module inclination, azimuth, and declination angle is given in (7) [19]. S_{module} is the incident solar irradiance (S_{incident}) calculated as the

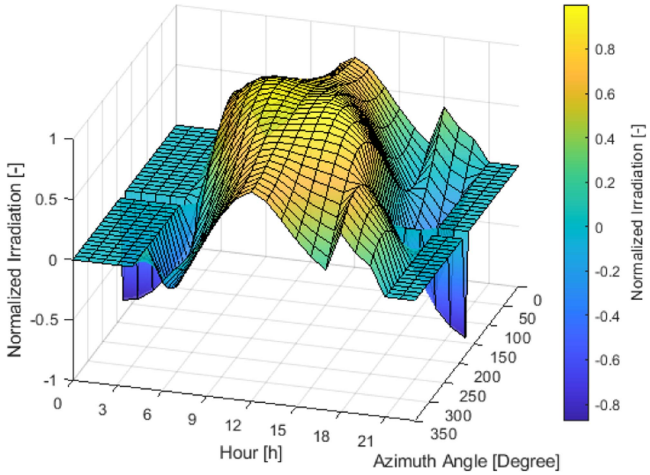

Fig. 1. Normalized solar radiation based on time and azimuth angle.

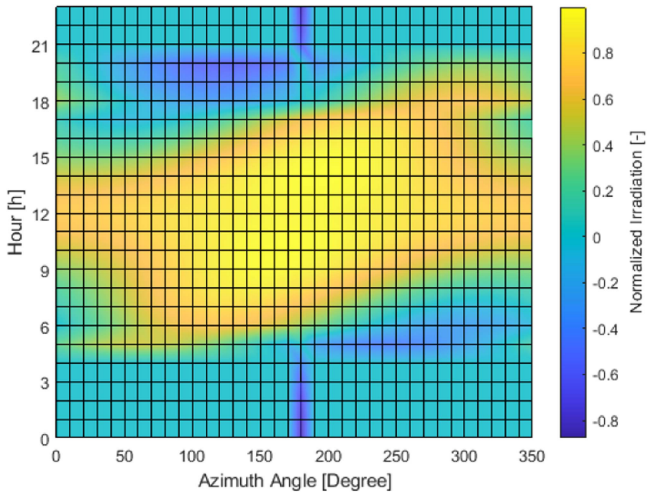

Fig. 2. Normalized solar radiation heat map.

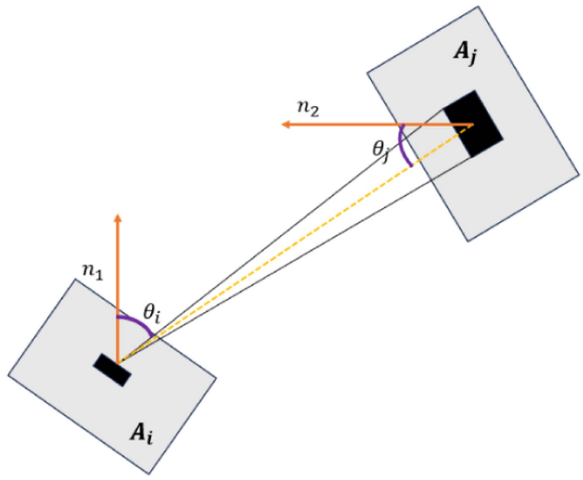

Fig. 3. Configuration of view factor.

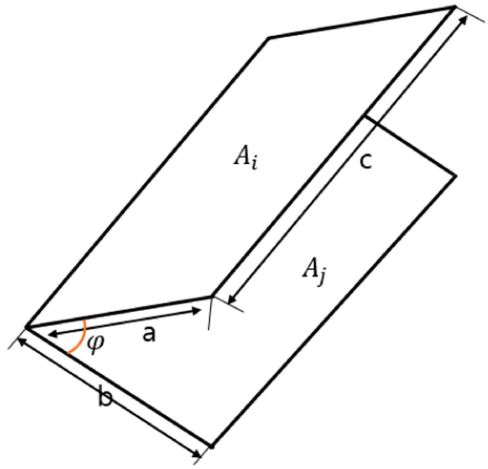

Fig. 4. Two rectangles with one common edge including the angle φ.

amount of sunlight incident vertically on the PV module. Meanwhile, $\Delta\beta$ represents the difference in azimuth angle between the position of the Sun and the installed PV module.

Figs. 1 and 2 represent the normalized solar radiation based on measurement time and azimuth angle. The increasing intensity of the orange color indicates higher solar radiation during specific times of the day. It is evident that solar radiation increases as the azimuth angle increases. This suggests that solar radiation and electricity generation can be adjusted based on azimuth angle to align with electricity consumption patterns.

B. Prediction of the Output of Bifacial PV Module

Bifacial PV modules generate power on both their front and rear surfaces, resulting in higher output compared to conventional single-sided PV modules, thanks to the additional power generated from the rear side. To predict the output of bifacial PV modules, we consider the predicted incident solar irradiance, predicted rear solar irradiance using the view factor theory, measured standard test condition (STC) output of the PV module, and module temperature.

A crucial aspect in predicting the output of bifacial PV modules is accurately estimating rear-side solar irradiance. This is achieved by utilizing the ground view factor and albedo (Alb) of the rear environment to comprehensively and precisely predict rear-side solar irradiance

$$F_{i\to j} = \frac{1}{A_i}\int_{A_j}\int_{A_i}\frac{\cos\theta_i\cos\theta_j}{\pi S^2}dA_i dA_j. \tag{8}$$

The view factor, which calculates the degree of radiation reaching one surface to another, is given in (8) [19].

The necessary variables for the view factor are shown in Fig. 3. The method proposed by Cha et al. [20], Feingold et al. [21], Hamilton and Morgan [22] applies this concept to PV power plants. The accuracy of the rear solar irradiance calculated using this theory was validated by measuring the rear solar irradiance of a system installed facing southward.

In Fig. 4, a constant angle (φ) is formed between the PV module and the ground. The lengths a and c represent the solar module's vertical and horizontal dimensions, respectively, while b denotes the distance influencing the reflection on the rear side where the module is installed. This distance is assumed to be

TABLE I
VIEW FACTOR ACCORDING TO THE INCLINATION ANGLE OF THE PV MODULE

Inclination Angle of PV Module [°]	View Factor [-]
15	0.121
30	0.153
45	0.135
60	0.107

equal to the length of two PV modules.

$$A = a/c$$
$$B = b/c$$
$$C = A^2 + B^2 - 2AB\cos\varphi$$
$$D = \left(1 + A^2\sin^2\varphi\right)^2. \tag{9}$$

Terms A, B, C, and D in (9) are defined to simplify the view factor equation.

$$\begin{aligned} F_{A_j \to A_i} &= -\frac{\sin 2\varphi}{4\pi B}\left[AB\sin\varphi + \left(\frac{\pi}{2} - \varphi\right)\left(A^2 + B^2\right)\right. \\ &\quad + B^2\tan^{-1}\left(\frac{A - B\cos\varphi}{B\sin\varphi}\right) + A^2\tan^{-1}\left(\frac{B - A\cos\varphi}{A\sin\varphi}\right)\Bigg] \\ &\quad + \frac{\sin^2\varphi}{4\pi B}\left\{\frac{2}{\sin^2\varphi} - 1\right\}\ln\left[\frac{\left(1 + A^2\right)\left(1 + B^2\right)}{1 + C}\right] \\ &\quad + B^2\ln\left[\frac{B^2\left(1 + C\right)}{\left(1 + B^2\right)C}\right] \\ &\quad + A^2\ln\left[\frac{A^2(1 + A^2)^{\cos 2\varphi}}{C(1 + C)^{\cos 2\varphi}}\right]\Bigg\} + \frac{1}{\pi}\tan^{-1}\left(\frac{1}{B}\right) \\ &\quad + \frac{A}{\pi B}\tan^{-1}\left(\frac{1}{A}\right) \\ &\quad - \frac{\sqrt{C}}{\pi B}\tan^{-1}\left(\frac{1}{\sqrt{C}}\right) + \frac{\sin\varphi\sin 2\varphi}{2\pi B}AD\left[\tan^{-1}\left(\frac{A\cos\varphi}{D}\right)\right. \\ &\quad \left. + \tan^{-1}\left(\frac{B - A\cos\varphi}{D}\right)\right] \\ &\quad + \frac{\cos\varphi}{\pi D}\int_0^B \sqrt{1 + \zeta^2\sin^2\varphi}\left[\tan^{-1}\left(\frac{\zeta\cos\varphi}{\sqrt{1 + \zeta^2\sin^2\varphi}}\right)\right. \\ &\quad \left. + \tan^{-1}\left(\frac{A - \zeta\cos\varphi}{\sqrt{1 + \zeta^2\sin^2\varphi}}\right)\right] d\zeta. \end{aligned} \tag{10}$$

Using (10), the view factor between the ground and the PV module can be calculated. The resulting values, depending on the inclination angle of the PV module, are listed in Table I.

The calculated view factor varied with the inclination angle of the PV module, with the largest value at 30°. As the inclination angle increased further, the view factor decreased, indicating a decrease in incident solar irradiance on the rear side.

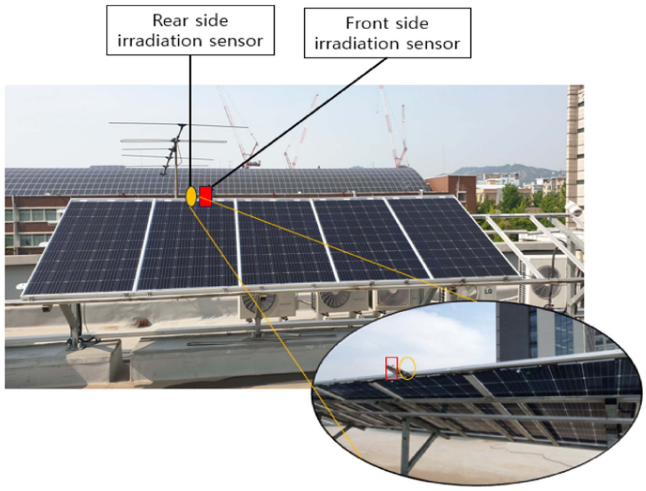

Fig. 5. Pyranometers installed on the front and rear sides of the module.

TABLE II
ANALYSIS OF ACCURACY BETWEEN MEASURED AND PREDICTED SOLAR IRRADIANCE

Measured Rear side Solar Irradiance $[W/m^2]$	Calculated Rear side Solar Irradiance $[W/m^2]$	Rear side MAPE [%]	Rear side RMSE $[W/m^2]$
138	122.67		
148	138.14		
158	154.83	5.05	9.26
172	172.75		

The rear solar irradiance, denoted by $S_{\text{rear\_direct}}$, represents the amount of solar irradiance directly reflected from the ground to the rear side of the module, and is estimated in the following equation:

$$S_{\text{rear\_direct}} \cong S_{\text{front}} \cdot \text{VF} \cdot \text{Alb}. \tag{11}$$

In (11), VF stands for view factor and Alb represents the albedo of the ground surface [19]. The measured albedo at the location where the experiment took place yielded a value of 0.08.

To validate the accuracy of the view factor theory, Fig. 5 displays a photograph of a bifacial PV power plant installed at 30°. The actual rear solar irradiance, measured at the site, was compared with the calculated solar irradiance for verification. Mean absolute percentage error (MAPE) and root mean square error (RMSE) were used for accuracy verification.

Table II presents the accuracy of the prediction model for rear-side solar irradiance using the data measured at the empirical site in Fig. 5. The results showed a MAPE of 5.05% and a RMSE of 9.26. The output of a bifacial PV module is the sum of the outputs from the front and rear sides, as shown in the following equation:

$$P_{\text{bifacial}} = P_{\text{front}} + P_{\text{rear}}. \tag{12}$$

TABLE III
380[W] BIFACIAL PV MODULE

Data	Front	Rear
Power [W]	380	275
I_{sc} [A]	10.05	7.38
V_{oc} [V]	48.29	47.78
Efficiency [%]	17.05	12.37
Temperature Coefficient [%/K]	0.37	–

The solar irradiance on the rear side, which considers both direct solar irradiance due to the view factor and the part determined by the Alb of the rear side where the PV module is installed, is represented in the following equation [19]:

$$P_{\text{bifacial}} = \left(\frac{S_{\text{front}}}{1000} \cdot P_{\text{front,STC}} + \frac{S_{\text{rear}_{\text{direct}}}}{1000} \cdot P_{\text{rear,STC}} \right) \cdot (1 + \delta_{P_{\text{mpp}}}(T_{\text{mod}} - 25)) \quad (13)$$

The bifacial PV module output calculation formula is presented in (13): P_{bifacial} represents the output power of the bifacial PV module, whereas $P_{\text{front,STC}}$ and $P_{\text{rear,STC}}$ refer to the measured values of the front and rear sides, respectively, under STC (AM 1.5G, 1000 [W/m^2], 25 °C). S_{front} represents the measured solar irradiance on the front side. $\delta_{P_{\text{mpp}}}$ refers to the temperature coefficient that affects the change in output due to temperature, where T_{mod} is the measured temperature of the PV module.

III. EXPERIMENT

An accuracy analysis was conducted by comparing the measured values from the outdoor experiments with those of the prediction model to apply an output prediction formula to PV power plants with various inclinations and azimuth angles.

A. Experimental Method

1) Measured and Predicted Output According to the Inclination Angle: First, experiments were conducted to validate the prediction equation based on the module inclination angle. The output was measured while varying the module inclination angle at fixed azimuths of 15°, 30°, 45°, and 60°. The experiment took place on the rooftop of Konkuk University (37.54°N,127°W), South Korea. To facilitate comparison between different systems, the measured data were normalized by dividing them by the system's capacity. The specifications of the PV modules used in the experiments are provided in Table III.

Experiments were conducted at inclination angles of 15°, 30°, 45°, and 60° with two bifacial PV modules facing azimuths of 90° and 270°. Figs. 6 and 7 show the experiments conducted at inclination angles of 15° and 60°.

Two bifacial PV modules with different azimuth angles were connected to separate inverters. This decision was made due to the variations in peak output times resulting from the different azimuth angles. Connecting the two systems directly could lead to output reduction due to output imbalance. To accurately capture this scenario, two measuring devices were utilized to collect the output data for each module. The prediction is made by calculating $S_{\text{horizontal}}$ using the measured irradiance and substituting it into the output prediction equation.

TABLE IV
PREDICTION ERROR RATES BY INCLINATION ANGLES

Inclination Angle [°]	Capacity [W]	MAPE [%]	RMSE [W]	RER [%]
15	325	9.54	10.61	3.26
30	325	9.08	10.31	3.17
45	325	7.92	11.33	3.49
60	325	11.55	14.90	4.58

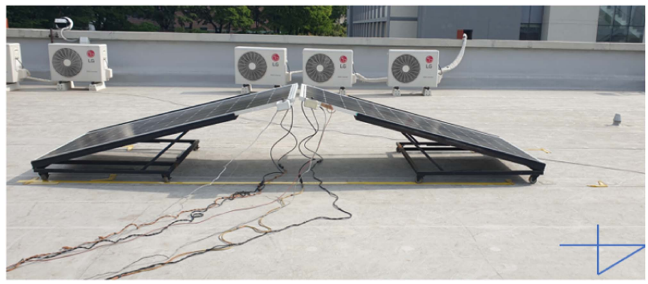

Fig. 6. Experiment with azimuth angles of 90° and 270°, with the inclination angle of 15°.

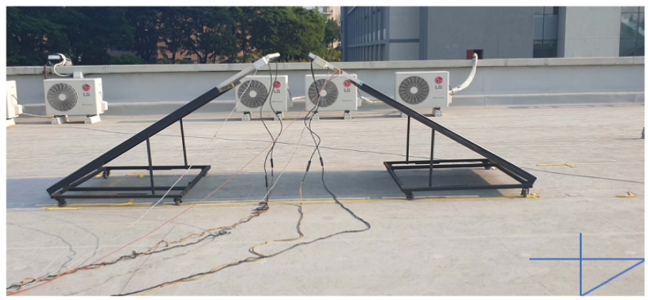

Fig. 7. Experiment with azimuth angles of 90° and 270°, with the inclination angle of 60°.

Verification of accuracy is crucial for the usability of the prediction. To assess accuracy, three error calculation methods were employed: MAPE, RMSE, and relative error rate (RER) methods. For the system with PV modules installed at 15°, the MAPE was found to be 9.54% and the RMSE was 10.61%. This error is believed to be due to relatively high errors during low-irradiance hours, such as after 16:00. To express this error based on the capacity of the PV module, the RER was defined using RMSE. RMSE represents the deviation between the actual and predicted values, which is an absolute numerical error. By dividing this value by the capacity of the module, it allows for interpretation as an error relative to the module capacity. The RER values for the modules installed at 15°, 30°, 45°, and 60° were 3.26%, 3.17%, 3.49%, and 4.45%, respectively. These RER values indicate the relative accuracy of the predictions considering the module capacity.

Fig. 8. Experiment with the inclination angle of 30°, with azimuth angles of 240° and 60°.

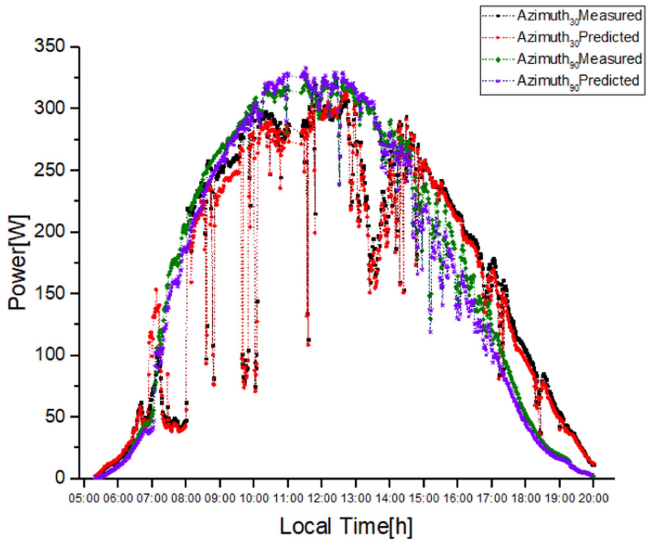

Fig. 9. Measured and predicted outputs with azimuth angles of 30° and 90°.

2) Prediction of Power Output With Installation Azimuth: For the experiments involving azimuthal changes, marks were placed on the ground at 30° intervals at the same experimental location. The PV modules installed facing east were rotated from an azimuth of 90° in increments of 30° toward the north. In contrast, the PV modules installed facing west were rotated from an azimuth of 270° in increments of 30° toward the south. This setup allowed for a systematic evaluation of the impact of azimuthal changes on the output of the PV modules. Fig. 8 shows the experiments conducted at an inclination angle of 30° with azimuthal angle of 240° and 60°.

Fig. 9 shows the results of measuring the output after fixing the inclination angle of the PV module at 30° and rotating the installation azimuth at intervals of 30°, along with the results calculated using the theoretical equations. In the figures, the *x*-axis represents the measurement time, and the *y*-axis represents the output according to the azimuth angle based on north (0°). The numbers next to the azimuth in the figure indicate the azimuth angles.

Table V presents the prediction errors based on the installation azimuth. The error between the results of the experiments conducted while changing the installation azimuth and the prediction value was found to be the lowest when the module was installed facing true east. Conversely, the error was highest at 240°. This difference in error can be attributed to higher inaccuracies during the morning hours when the Sun is in the east. In addition, the output of the west-facing PV modules was relatively small due to factors such as the view factor on the rear and the direct irradiance entering from the rear. Overall, the output prediction based on azimuth had a prediction error of approximately 5%.

TABLE V
PREDICTION ERROR RATES WITH INSTALLATION AZIMUTHS

Azimuth Angle [°]	Capacity [W]	MAPE [%]	RMSE [W]	RER [%]
30	325	5.71	11.18	3.44
60	325	17.79	25.59	5.47
90	325	8.55	10.74	3.30
210	325	23.62	19.12	5.88
240	325	17.73	24.54	7.55
270	325	14.94	21.96	6.76

Fig. 10. Large-scale PV power plant installed at azimuth the angles of 122° and 302°.

3) Verification at Large-Scale Solar Power Plant: The output was predicted based on the installation azimuth and inclination angle of a small-scale power plant, and the results were analyzed and presented. Using these results, the irradiance and output predictions of a large-scale PV power plant were performed to improve the stability of the actual grid.

Fig. 10 shows an overview of a large-scale PV power plant in Nonsan, South Korea (36.15°N,127°W) used in the analysis. The power plant was installed facing 122° eastward and 302° westward from 0° north. Data were collected from inverters installed in both eastward and westward directions. In addition, to compare the predicted solar irradiance and output, data measured with a pyranometer were used, and the output to the inverter was used for analysis.

Fig. 11 shows a comparison between the predicted and actual values of solar irradiance by taking the hourly average using data from May 10 to June 9, when the small-scale solar power plant experiment was conducted. The predicted and actual values exhibited the same pattern across all intervals. An error analysis was conducted to accurately compare these results.

Table VI presents the results of the irradiance prediction error analysis for the large-scale PV power plant. On May 10, the

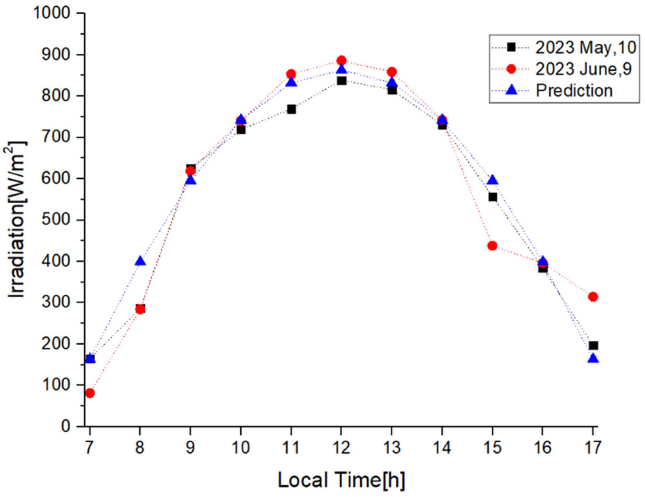

Fig. 11. Comparison with predicted solar irradiance and measured data on May 10 and June 9, 2023.

TABLE VI
ANALYSIS OF IRRADIANCE PREDICTION ERRORS AT LARGE-SCALE PV POWER PLANT

Date	MAPE [%]	RMSE [W]	RER [%]
May 10	3.56	37.93	3.79
June 9	4.85	39.37	3.93

TABLE VII
ANALYSIS OF OUTPUT PREDICTION ERRORS AT LARGE-SCALE SOLAR POWER PLANT

Date	MAPE [%]	RMSE [W/m^2]	RER [%]
May 10	8.19	44.49	4.45
June 9	9.59	79.57	7.96

MAPE, RMSE, and RER values were 8.19%, 44.49 W/m^2, and 4.45%, respectively. The error was within 5% of the measured data, which was not significantly different from the error predicted for a small-scale PV power plant. Conversely, the data for June 9 showed MAPE, RMSE, and RER values of 9.59%, 79.57 W/m^2, and 7.96%, respectively. The error was relatively high (7.96%) compared to the measured data. This was because the accuracy was relatively low owing to large variations in irradiance caused by clouds on the day of measurement when the output decreased due to cloud cover. This is because the predictions use the theoretically calculated irradiance. Therefore, RER was conducted to objectively compare the results.

The results of the output prediction error analysis for the large-scale PV power plant are as follows: On May 10, the MAPE, RMSE, and RER values were 3.56%, 37.93 W, and 3.79%, respectively. On June 9, the MAPE, RMSE, and RER were 4.85%, 39.37 W, and 3.93%, respectively. Therefore, because the output prediction error rate is less than 5%, this method can be used in both small- and large-scale solar power plants. In the next section, this is used to conduct research on system stability.

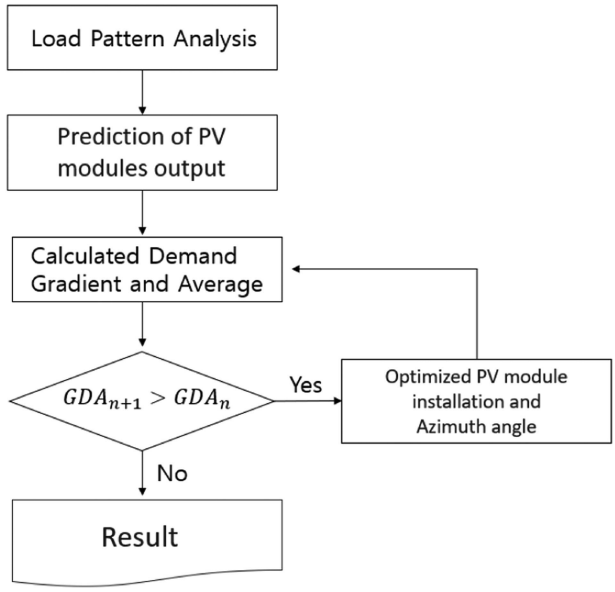

Fig. 12. Optimization flow chart of the installation of PV modules according to load pattern.

IV. APPLICATIONS

Electricity usage in Metropolitan Seoul falls into categories like residential, public, service, or manufacturing, each with unique consumption patterns. Consequently, there are periods of electricity usage spikes, negatively impacting the electrical supply stability. To address this, installing solar power plants can help mitigate these peaks by providing additional electricity supply during high-demand periods.

Fig. 12 shows a flowchart for optimizing the power system stability by PV module inclination and azimuth angle. Using this method, a PV module installation method suitable for each household and industrial power usage pattern was presented.

A. Demand Gradient (DG) and Average According to Electrical Usage Patterns

PV power systems represent eco-friendly energy sources that contribute to achieving RE100 goals. They harness the Sun's infinite energy to generate electricity without concerns of depletion. However, a drawback is their dependency on daylight for power generation. To maximize electricity production during daylight hours, installation methods that yield peak power output have been adopted. Yet, this approach causes challenges in the power grid, leading to the "duck curve" phenomenon.

The duck curve refers to a situation in power systems where electricity usage decreases due to high solar power production during peak generation times. However, during periods of low solar power production, solar energy cannot fully compensate for power usage, leading to high grid power consumption. This

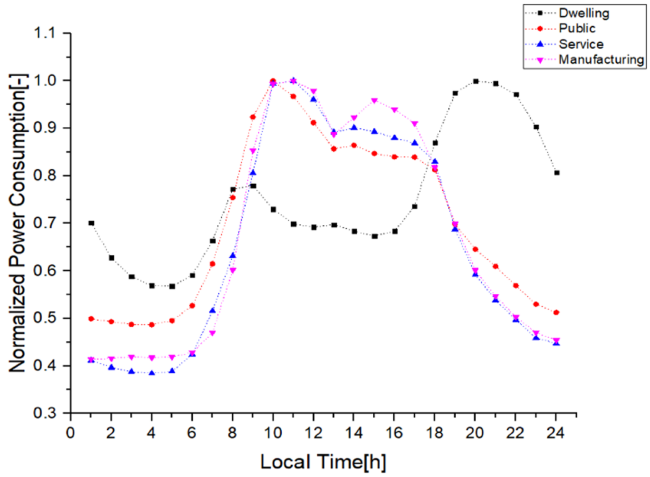

Fig. 13. Load patterns for representative industries in metropolitan Seoul.

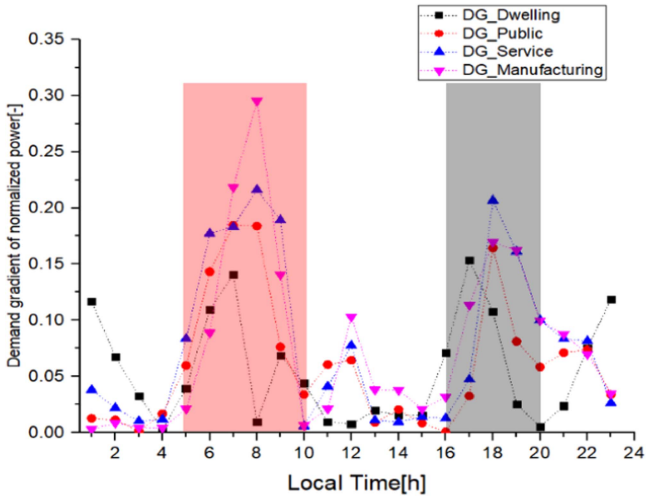

Fig. 14. Variation of DG of electricity usage in metropolitan Seoul.

rapid fluctuation in the power grid can destabilize the system. To address this issue, different PV power plant installation methods have been investigated to analyze the power change rate in the power grid. The goal is to find installation strategies that can better match power generation with electricity usage patterns and mitigate the impact of the duck curve phenomenon.

Fig. 13 shows the normalized load patterns for the representative industries in Metropolitan Seoul. Based on these patterns, intervals of increased electricity consumption can be identified. Residential, public, service, and manufacturing consumption vary according to commuting hours and activity times. To analyze these load patterns, we utilize the DG, which is defined as the rate of change in power usage over time.

$$DG_n = \frac{\Delta P}{\Delta t} = \frac{P_n - P_{n-1}}{t_n - t_{n-1}}. \tag{14}$$

DG is a method used to represent changes in the amount of power that is either burdened or alleviated in a power system.

This can be expressed in (14), which is calculated as the ratio of the change in power usage to the change in time. The change in the DG for each power usage method is shown in Fig. 14, with the times of abrupt changes in power usage marked with red and black boxes.

$$P_n = \text{Electricity demand} - \text{PV generation}. \tag{15}$$

Equation (15) represents a formulation of Power (P) defined in (14). This signifies the reduction in power consumption due to solar generation from the total electricity usage. DG can be defined as the decreased electricity usage resulting from time-varying PV generation

$$\text{DGA} = \frac{1}{24}\sum_{n=1}^{24} DG_n. \tag{16}$$

The installation method of the PV modules for minimizing the load change rate in the power grid was analyzed using (16). The values calculated through the DG were averaged over 24 h, and this average was compared to derive the demand gradient

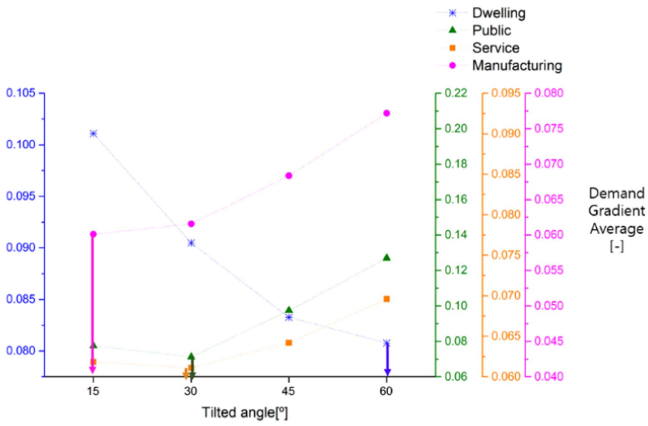

Fig. 15. Variation of DGA with inclination angles (inclination angles).

average (DGA). DGA is a metric that indicates the quality of variation. A DGA close to 0 signifies small variations that are considered favorable, whereas a DGA close to 1 indicates large variations that are considered unfavorable.

B. Variation of DGA With Inclination Angles

The azimuth angle was fixed, and only the inclination angle was altered to compare the changes in the DGA based on the inclination angle.

Fig. 15 shows the changes in the DGA based on the inclination angle for each electrical usage pattern. For residential use (dwellings), as the inclination angle increased, the variation decreased, with the lowest variation at 60°. The public, service, and manufacturing sectors showed different variations and exhibited the most favorable values at inclination angles of 30°, 30°, and 15°, respectively.

C. Variation of DGA With Installation Azimuths

In Fig. 16, an analysis of the changes in the DGA based on the module installation azimuth is presented. For the dwelling,

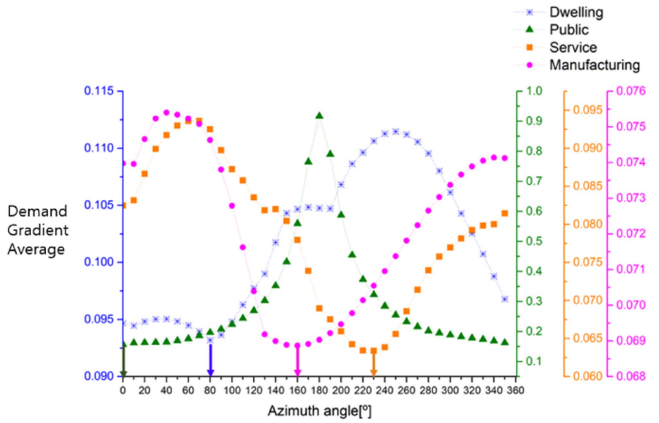

Fig. 16. Variation of DGA with installation azimuths.

TABLE VIII
OPTIMAL INCLINATION ANGLE AND AZIMUTH ACCORDING TO LOAD PATTERN

Category of electricity usage	Optimal inclination angle [°]	Optimal installation azimuth [°]	DGA
Dwelling	60	330	0.05700
Public	60	210	0.05051
Service	35	230	0.05136
Manufacturing	50	190	0.05528

public, service, and manufacturing sectors, the optimal installation azimuth angles were found to be 0°, 80°, 160°, and 230°, respectively. The power data used for this analysis were obtained from Metropolitan Seoul, situated at 37.54°N and 127°W.

While the maximum output of the PV module was achieved when facing south (180°) considering the solar path at this location, the DGA results based on the azimuth angle indicate that facing south is not the optimal installation method from a power-grid stabilization perspective for all demands, except for the manufacturing sector. The public sector, in particular, exhibited the worst results in terms of power grid stability.

These findings suggest that an inclination angle at 180° should be avoided to ensure power-grid stability in cities where the public sector constitutes the main business structure.

D. Variation of DGA With Inclination Angles and Azimuths

The optimal inclination angle and azimuth based on the load patterns were analyzed, and the results are plotted in Figs. 17–20. The *x*-axis represents the inclination angle (inclination angle) and the *y*-axis represents the azimuth angle. Closer to blue indicates a DGA value closer to 0, which is favorable, whereas closer to red signifies a DGA value closer to 1. The optimal installation for grid stability can be achieved by installing under one of the conditions in the blue area.

Table VIII lists the optimal inclination angle and azimuth according to load patterns. The optimal inclination angle was found to be 30° or above, while the optimal azimuths for residential use were northwest and southwest for the public, service, and

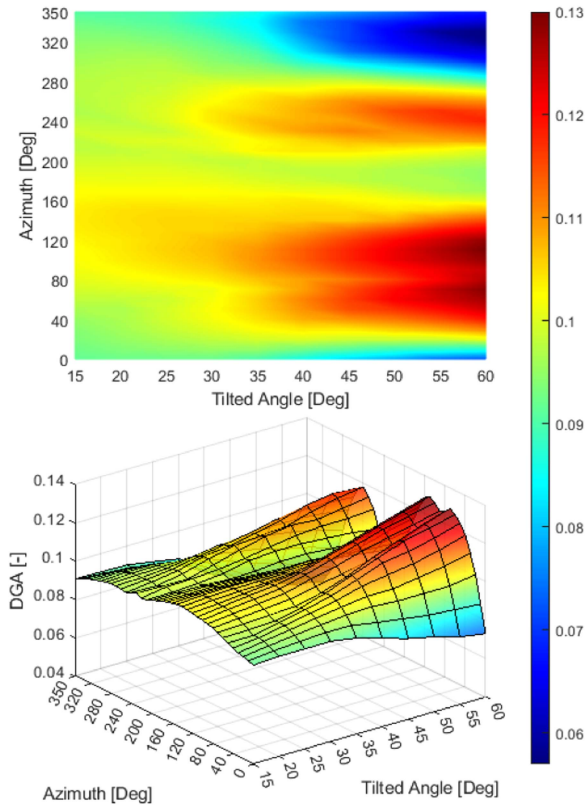

Fig. 17. Variation of DGA with inclination and azimuth angles in the dwelling sector.

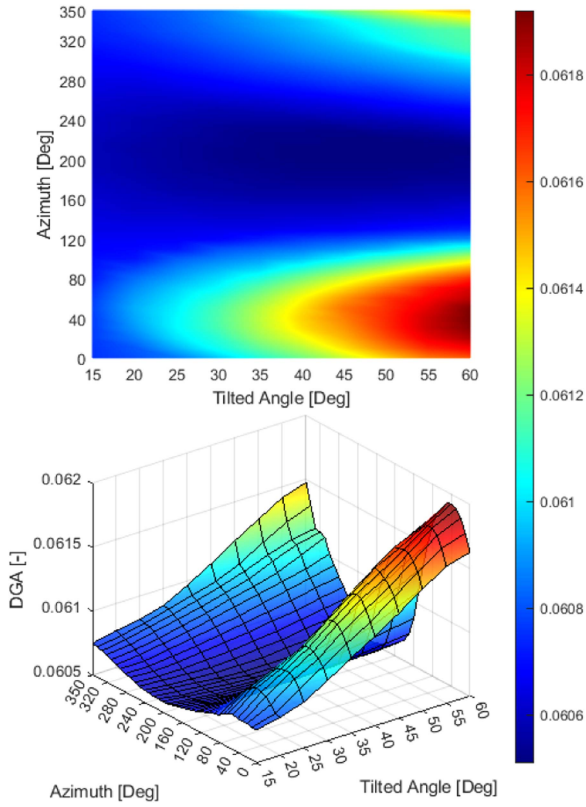

Fig. 18. Variation of DGA with inclination and azimuth angles in the public sector.

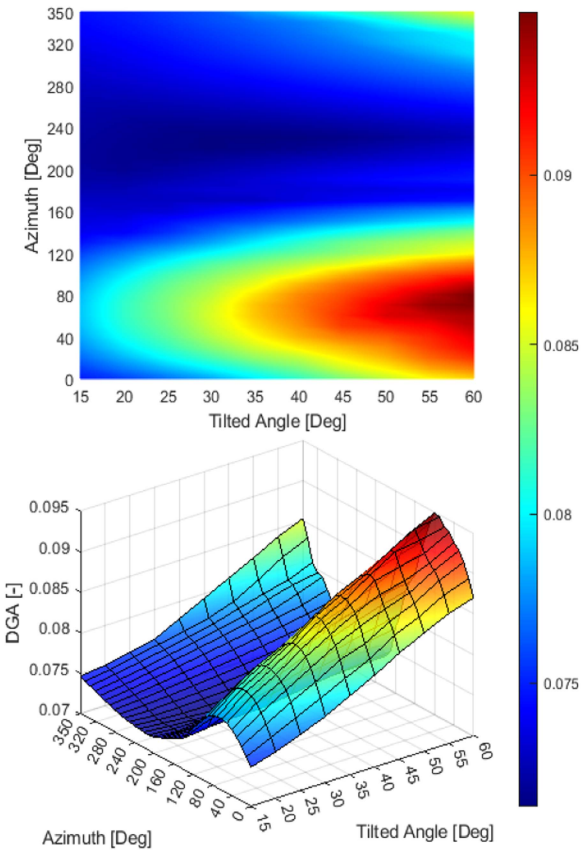

Fig. 19. Variation of DGA with inclination and azimuth angles in the service sector.

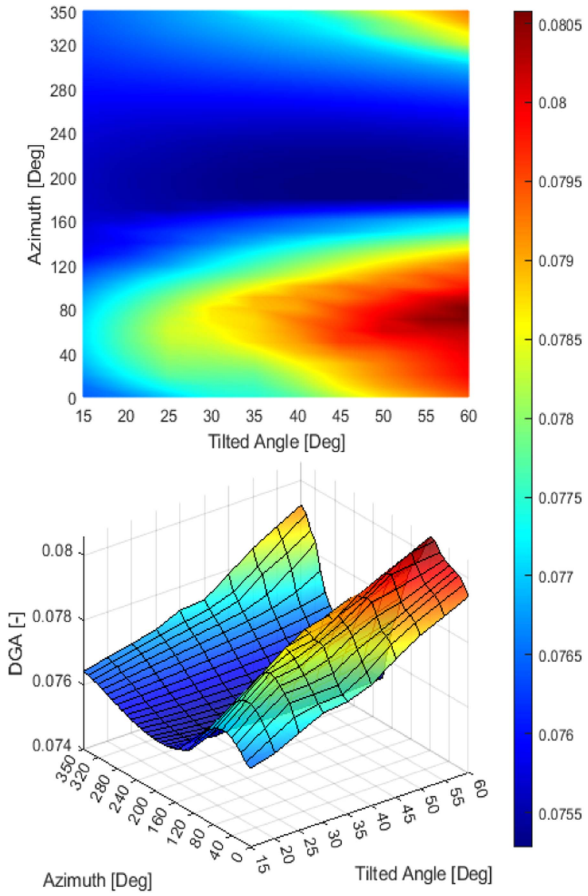

Fig. 20. Variation of DGA with inclination and azimuth angles in the manufacturing sector.

manufacturing sectors. This suggests that different installation methods have to be selected for different load patterns. By applying installation methods that correspond to the load patterns of the main businesses in a city, grid stability could be improved.

V. Result

In this section, the actual changes in electricity usage of the transmission lines were analyzed when the PV module inclination angles and orientations for each electricity usage pattern presented in Section IV were applied.

Figs. 21–24 represent the cases of south-facing installation and those where the DGA is minimized. The black square labeled "Power consumption" in the figures represents the normal case, indicating the typical electricity usage pattern when a PV power plant has not been applied. The red circle signifies the scenario when installed facing south to achieve maximum electrical output. The blue triangle represents the grid stability installation case, which illustrates the electricity usage pattern when installed in a manner that minimizes the DGA, as presented in Table VIII.

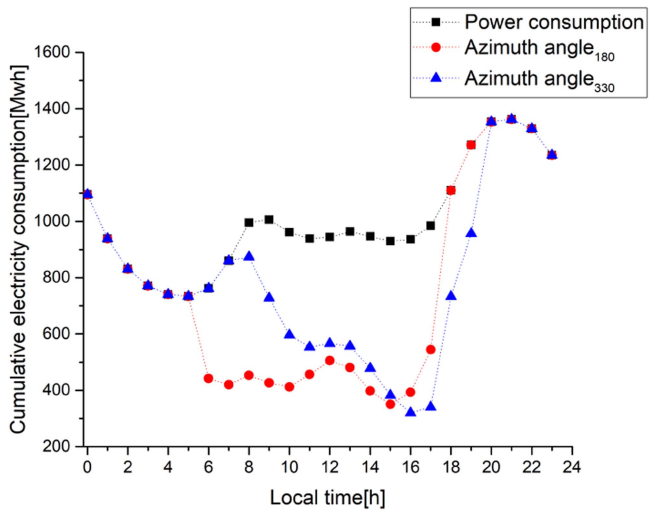

Fig. 21. DGA for dwelling case.

Fig. 21 illustrates the changes in the electricity pattern for the Dwelling case. When installed facing south (red circle), it is observed that the electricity generation is high, resulting in the lowest amount of electricity supplied through the grid. In contrast, the grid stability case (blue triangle) has a lower output compared to the south-facing installation, but it can be seen that the rate of change in electricity consumption is relatively reduced. In the Dwelling case, the DGA was 0.1009 and after the adjustments in the installation, the improved DGA is 0.057. This represents a 77.02% improvement in power stability.

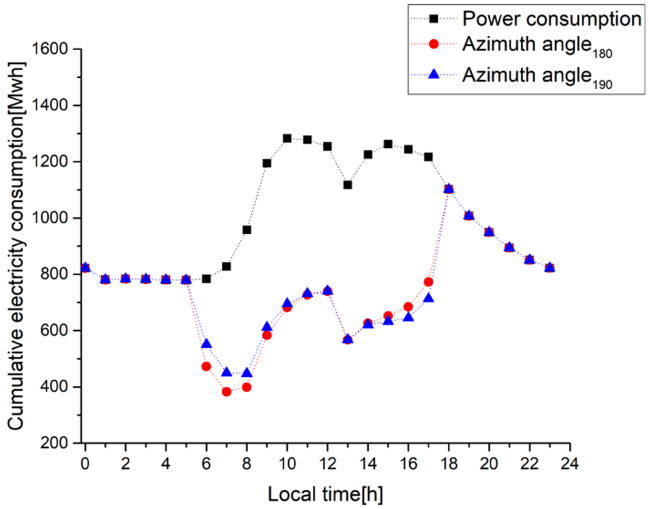

Fig. 22. DGA for manufacturing case.

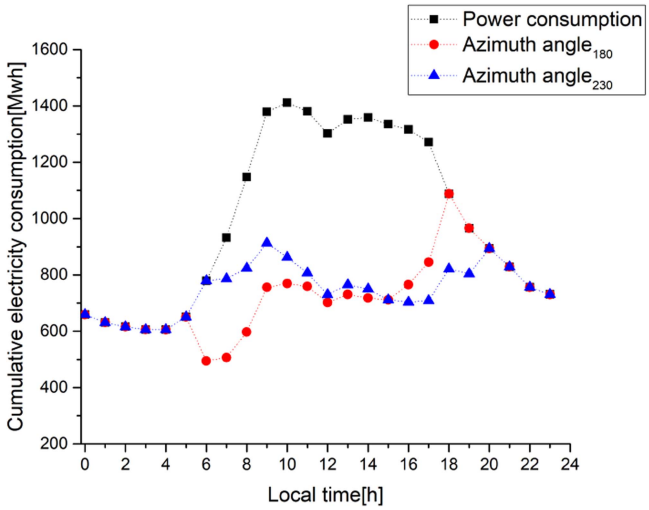

Fig. 24. DGA for service case.

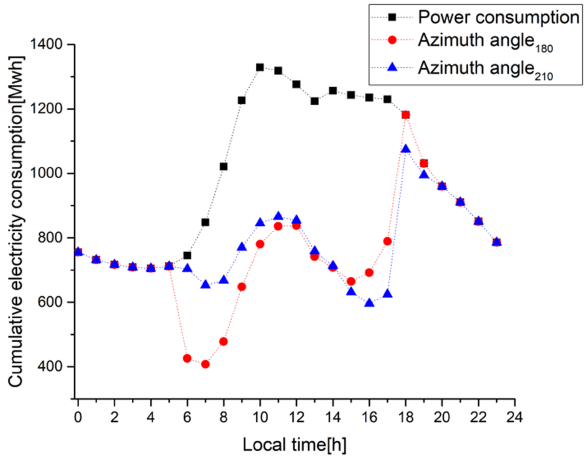

Fig. 23. DGA for public case.

Fig. 22 depicts the change in the electricity usage pattern for the Manufacturing case. In this scenario, the south-facing installation (red circle) and the angle that results in the minimum DGA (blue triangle) differ by only 10°. Therefore, for manufacturing, the installation method that generates the maximum amount of electricity does not significantly differ from the grid stability case. As a result, in areas predominantly composed of manufacturing industries, south-facing installation is the most advantageous approach.

Fig. 23 shows the change in the electricity usage pattern for the Public case. In this case, the south-facing installation (red circle) tends to decrease the stability of the power grid due to the amount of electricity generated in the morning hours. Although the generation between 14:00 and 16:00, and after 18:00, are higher at the grid stability case (blue triangle), it shows more gradual change compared to the south-facing case. Therefore, the grid stability case results in higher stability of the power grid.

Fig. 24 shows the change in the electricity usage pattern for the Service case. In the grid stability case (blue triangle), the output after 16:00 is observed to be higher compared to the south-facing (red circle) direction, and the rate of change throughout the generation time is relatively low, indicating that the stability of the power grid is high. The DGA was 0.07324, and after adjustments made through installation, the improved DGA was 0.05136. This represents a 42.6% improvement in power stability.

This analysis indicates that the installation azimuth angle can influence the stability of the power grid according to the electricity usage pattern, and these results demonstrate that adjusting the installation methods of PV modules according to the predominant industries of each city would be beneficial for power grid stability.

VI. Conclusion

RE100 represents a global commitment to a sustainable future, and large-scale PV power systems are being widely installed to maximize power generation and meet this commitment. First, solar radiation was calculated based on the inclination and azimuth angle to predict the output of bifacial solar modules. The calculated output was compared with actual measurements from both small and large-scale solar power plants, resulting in a mean absolute percentage error (MAPE) of 5.71%. Using this output prediction model, the optimal inclination angles were analyzed for different electricity usage patterns. In the Dwelling case, the DGA value improved from 0.1009 to 0.057, a 77% enhancement. In the Public case, the DGA value improved from 0.06055 to 0.05, a 21.1% enhancement. For the Service case, it improved from 0.07324 to 0.05136, a 42.6% improvement, and in the Manufacturing case, it improved from 0.07538 to 0.05528, a 36.4% increase, indicating a high degree of stability improvement.

This research may not be applicable in countries with sufficient grid capacity or those where maximum output is not critical. However, it could be beneficial in countries facing grid capacity limitations and localized high-capacity installations, such as South Korea, to improve electrical stability.

REFERENCES

[1] K. Ju-Hee, K. Hyo-Jin, and Y. Seung-Hoon, "Willingness to pay price premium for smartphones produced using renewable energy," *MDPI Sustainability*, vol. 11, no. 6, Mar. 2019, Art. no. 1566, doi: 10.3390/su11061566.

[2] S. Ong, "Land-use requirements for solar power plants in the United States," Nat. Renew. Energy Lab. (NREL), Golden, CO, USA, Tech. Rep., NREL/TP-6A20-56290, 2013.

[3] M. Bolinger and G. Bolinger, "Land requirements for utility-scale PV: An empirical update on power and energy density," *IEEE J. Photovolt.*, vol. 12, no. 2, pp. 589–594, Mar. 2022, doi: 10.1109/JPHOTOV.2021.3136805.

[4] T. Sugiura, S. Matsumoto, and N. Nakano, "Bifacial PERC solar cell designs: Bulk and rear properties and illumination condition," *IEEE J. Photovolt.*, vol. 10, no. 6, pp. 1538–1544, Nov. 2020, doi: 10.1109/JPHOTOV.2020.3013987.

[5] R. Gautam, V. Rohit, and S. Sunanda, "Study on the optimum orientation of bifacial photovoltaic module," *Int. J. Energy Res.*, vol. 46, no. 4, pp. 4247–4266, Oct. 2021, doi: 10.1002/er.7423.

[6] R. Torabi, A. Gomes, and F. Morgado-Dias, "The duck curve characteristic and storage requirements for greening the Island of Porto Santo," in *Proc. Energy Sustainability Small Developing Economies*, 2018, pp. 1–7, doi: 10.1109/ES2DE.2018.8494235.

[7] P. N. Korovesis, G. A. Vokas, I. F. Gonos, and F. V. Topalis, "Influence of large-scale installation of energy saving lamps on the line Voltage distortion of a weak network supplied by photovoltaic station," *IEEE Trans. Power Del.*, vol. 19, no. 4, pp. 1787–1793, Oct. 2004, doi: 10.1109/TPWRD.2004.835432.

[8] A. Barbón, C. Bayón-Cueli, L. Bayón, and C. Rodríguez-Suanzes, "Analysis of the inclination and azimuth angles of photovoltaic systems in non-ideal positions for urban applications," *Appl. Energy*, vol. 305, Sep. 2021, Art. no. 117802, doi: 10.1016/j.apenergy.2021.117802.

[9] T. Baumann et al., "Photovoltaic systems with vertically mounted bifacial PV modules in combination with green roofs," *Sol. Energy*, vol. 190, pp. 139–146, Aug. 2019, doi: 10.1016/j.solener.2019.08.014.

[10] T. Khatib and R. Deria, "East-west oriented photovoltaic power systems: Model, benefits and technical evaluation," *Energy Convers. Manage.*, vol. 266, May 2022, Art. no. 115810, doi: 10.1016/j.enconman.2022.115810.

[11] O. Y. Rahimat, T. M. Ankoh, D. L. Mensah, A. D. Quansah, and S. M. Adaramola, "Predicting the potential energy yield of bifacial solar PV systems in low-latitude region," *Energies*, vol. 15, no. 22, Nov. 2022, Art. no. 8510, doi: 10.3390/en15228510.

[12] R. Abdallah, A. Juaidi, S. Abdel-Fattah, and F. Manzano-Agugliaro, "Estimating the optimum inclination angles for south-facing surfaces in Palestine," *Energies*, vol. 13, no. 3, pp. 9–15, Jan. 2020, doi: 10.3390/en13030623.

[13] W. C. L. Kamuyu, J. R. Lim, C. S. Won, and H. K. Ahn, "Prediction model of photovoltaic module temperature for power performance of floating PVs," *Energies*, vol. 11, no. 2, 2018, Art. no. 447, doi: 10.3390/en11020447.

[14] G. G. Kim et al., "Prediction model for PV performance with correlation analysis of environmental variables," *IEEE J. Photovolt.*, vol. 9, no. 3, pp. 832–841, May 2019, doi: 10.1109/JPHOTOV.2019.2898521.

[15] A. George and R. Anto, "Analytical and experimental analysis of optimal inclination angle of solar photovoltaic systems," in *Proc. Int. Conf. Green Technol.*, 2012, pp. 234–239, doi: 10.1109/ICGT.2012.6477978.

[16] S. F. A. Shah, I. A. Khan, and H. A. Khan, "Performance evaluation of two similar 100MW solar PV plants located in environmentally homogeneous conditions," *IEEE Access*, vol. 7, pp. 161697–161707, 2019, doi: 10.1109/ACCESS.2019.2951688.

[17] W. Chun-Sheng, W. Yi-Bo, L. Si-yang, P. Yan-chang, and X. Hong-Hua, "Study on automatic sun-tracking technology in PV generation," in *Proc. 3rd Int. Conf. Electric Utility Deregulation Restructuring Power Technol.*, 2008, pp. 2586–2591, doi: 10.1109/DRPT.2008.4523847.

[18] I. Dincer, *Comprehensive Energy Systems*. Amsterdam, The Netherlands: Elsevier, 2018.

[19] B. G. Bhang et al., "Optimal design of bifacial floating photovoltaic system with different installation azimuths," *IEEE Access*, vol. 11, pp. 1456–1466, 2023, doi: 10.1109/ACCESS.2022.3233100.

[20] H. L. Cha, B. G. Bhang, S. Y. Park, J. H. Choi, and H. K. Ahn, "Power prediction of bifacial Si PV module with different reflection conditions on rooftop," *Appl. Sci.*, vol. 8, no. 10, 2018, Art. no. 1752, doi: 10.3390/app8101752.

[21] A. Feingold and K. G. Gupta, "New analytical approach to the evaluation of configuration factors in radiation from spheres and infinitely long cylinders," *J. Heat Transfer*, vol. 92, no. 1, pp. 69–76, 1970.

[22] D. C. Hamilton and W. R. Morgan, "Radiant-interchange configuration factors," NASA TN 2836, 1952.

Hoonjoo Choi received the B.S. degree in environmental engineering from Yonsei University, Seoul, South Korea, in 2004, and the M.S. degree in electrical characteristics of solar modules using Tin bus-bars from Konkuk University, Seoul, where he is currently working toward the Ph.D. degree with Next Generation Photovoltaic Module and Power System Research Center.

His Ph.D. research focuses on digital operation and maintenance for photovoltaic power generation system improvement and health management in a variety of environments.

Jinho Choi received the B.S., M.S., and Ph.D. degrees in electrical engineering from Konkuk University, Seoul, South Korea, in 2018, 2019, and 2023, respectively.

He is currently with Chungbuk Techno Park (CBTP), Chungbuk, South Korea. His Ph.D. thesis is the prediction of output for high density modules. His research focuses on power prediction and fault detection of floating and marine photovoltaics using high-density PV modules (HDM) for RE100.

Seong-Hyeon Ahn received the B.S. degree from Konkuk University, Seoul, South Korea, in 2023, where he is currently working toward the M.S. degree in electrical engineering with the Next Generation Photovoltaic Module and Power System Research Center.

His research interests include PV power system diagnosis with power index and the fusion of renewable energy resources for RE100.

Jin Hee Hyun received the B.S. degree in electrical and electronic engineering from Konkuk University, Seoul, South Korea, in 2020, and the M.S. degree in electrical and electronic engineering from Next Generation Photovoltaic Module and Power System Research Center, Konkuk University, in 2022.

Her research interests include reliability of high power density PV module such as bifacial module and its application in floating and Marine PVs.

Hae-Lim Cha received the B.S. and M.S. degrees in electrical engineering, in 2015 and 2017, respectively, from Konkuk University, Seoul, South Korea, where she is currently working toward the Ph.D. degree in the Next Generation Photovoltaic Module and Power System Research Center.

he works with Korea Telecom. Her research interests include bifacial PV module and their application in BIPV systems.

Byeong-Yong Lim received the B.S. degree in electrical and electronic engineering from Hongik University, Seoul, South Korea, the M.S. degree in 2020 from Konkuk University, Seoul, where he is currently working toward the Ph.D. degree with the Next Generation Photovoltaic Module and Power System Research Center.

His research interests include reliability of solar cell, PV module and fault detection of power generation system of floating PVs.

Hyung-Keun Ahn (Member, IEEE) received the B.S. and M.S. degrees in MOSFETs in electrical engineering from Yonsei University, Seoul, South Korea, in 1983 and 1985, respectively, and the Ph.D. degree in HEMTs from the Department of Electrical Engineering, University of Pittsburgh, Pittsburgh, PA, USA, in 1993. From 1986 to 1995, he was with the LG Semiconductor Co. working on silicon-based device design and process integration. In 1995, he joined the Department of Electrical Engineering, Konkuk University, Seoul, South Korea, where he is a Professor and Dean of Next Generation PV Module and Power System R&D Center. From 2014 to 2016, he was also a Foreign Professor with the Department of Electrical and Control Engineering, Division of Electrical Engineering, Shandong University of Technology, Zibo, Shandong, China. He was the first National Photovoltaic Research and Development Program Director of the Ministry of Knowledge Economy, South Korea, from 2009 to 2011. He is currently working on fault detection of PV station and microgrid network design for net-zero energy environments using renewable energy resources including ESS, wind and fuel cell with floating and marine photovoltaic systems under the demand response control for RE100. His research interests include reliability of both Si and GaAs-based solar cells and PV modules for applications in micro roof-top to large scale of PVs connected with ESS and his key focuses stay on failure analysis, reliability, and maintenance, repair, and operation for durable renewable energy system.

Dr. Ahn was a Committee Member of the National Science and Technology Commission, Department of Energy, South Korea, from 2005 to 2007.